JACS
JOURNAL OF THE AMERICAN CHEMICAL SOCIETY

Article

pubs.acs.org/JACS

# Complete State-Resolved Non-Adiabatic Dynamics of the $O(^3P) + D_2 \rightarrow OD(X^2\Pi) + D$ Reaction

Sridhar A. Lahankar,[†] Jianming Zhang,[†] Timothy K. Minton,*[,†,‡] and Kenneth G. McKendrick*[,§]

[†]Department of Chemistry and Biochemistry, Montana State University, Bozeman, Montana 59717, United States

[‡]Research Fellow at State Key Laboratory of Molecular Reaction Dynamics, Dalian Institute of Chemical Physics, Chinese Academy of Sciences, 457 Zhongshan Road, Dalian, Liaoning 116023, China

[§]Institute of Chemical Sciences, School of Engineering and Physical Sciences, Heriot-Watt University, Edinburgh, EH14 4AS, U.K.

**ABSTRACT:** The first quantum-state-resolved distributions over the full range of available product levels are reported for any isotopic variant of the elementary reaction of $O(^3P)$ with molecular hydrogen. A laser-detonation source was used to produce a hyperthermal oxygen-atom beam, which allowed for sufficient collision energy to surmount the reaction barrier. This beam was crossed by a supersonic beam of $D_2$. The nascent OD products were detected by laser-induced fluorescence. OD rotational distributions in vibrational states $v' = 0$, 1, and 2 at a collision energy of 25 kcal mol$^{-1}$ are reported, together with distributions for the dominant product vibrational level, $v' = 0$, at lower collision energies of 20 and 15 kcal mol$^{-1}$. The OD product is highly rotationally excited, to a degree that declines as expected for the higher vibrational levels or for reductions in the collision energy. The measured rovibrational distributions at the highest collision energy are in excellent agreement with previous theoretical predictions based on quantum scattering calculations on the triplet potential energy surfaces developed by Rogers et al. (*J. Phys. Chem. A* **2000**, *104*, 2308−2325). However, no significant OD spin−orbit preference was observed, in contrast to the predictions of most existing theoretical models of the non-adiabatic dynamics based on the widely used reduced-dimensional four-state model of Hoffmann and Schatz (*J. Chem. Phys.* **2000**, *113*, 9456−9465). Furthermore, a clear observed preference for OD $\Pi(A')$ $\Lambda$-doublet levels is not consistent with a simple extrapolation of the calculated relative reaction cross sections on intermediate surfaces of $^3A'$ and $^3A''$ symmetry.

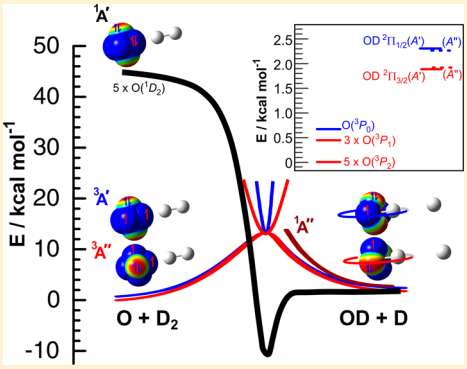


## 1. INTRODUCTION

Reaction with molecular hydrogen is, in terms of the number of electrons, the most fundamental reaction involving oxygen atoms. Despite this apparent simplicity, the reaction of ground-state $O(^3P)$ with molecular hydrogen is a key step in the combustion of hydrogen and hydrocarbon fuels.[1] It plays an important role in the chemistry of Earth's outer atmosphere and in hotter interstellar environments, such as photon-dominated regions of dense clouds close to hot stars[2] and in certain regions of proto-planetary disks.[3−5] Moreover, it is one of the benchmark triatomic reactions that have been treated theoretically for more than three decades.[6−32] However, for challenging practical reasons, it has largely eluded a parallel detailed experimental investigation.

Other triatomic benchmark reactions, most notably $H + H_2$ and $F + H_2$ (and their isotopologues), have a long history of detailed examination by both experiment and theory and continue to be scrutinized intensely.[33−36] Initially, the focus was primarily on the heavy-particle dynamics, but more recently interest has expanded into electronic effects. Breakdown of the Born−Oppenheimer approximation has been observed experimentally in the reaction $F + H_2$,[33] coinciding with a new wave of theoretical interest.[34,35] The reactivity of ground $F(^2P_{3/2})$ and excited $F(^2P_{1/2})$ spin−orbit states is affected by the non-adiabatic coupling between reactive and nonreactive potential energy surfaces (PESs) on the reactant side.

The $O(^3P) + D_2 \rightarrow OD(X^2\Pi) + D$ system, which is the subject here, represents an important and fundamentally more challenging class of reactions, because the fine-structure splittings are not confined to the reactant side. In this reaction, non-adiabatic coupling between multiple electronic PESs is possible throughout the reaction path. The spin−orbit interaction in $O(^3P)$ results in three fine-structure states, $^3P_2$, $^3P_1$, and $^3P_0$, with degeneracies of 5, 3, and 1, respectively. The successive energy splittings are 158 and 69 cm$^{-1}$ (equivalent to 0.45 and 0.20 kcal mol$^{-1}$). Disregarding for the moment spin−orbit coupling, the 9-fold asymptotic degeneracy maps onto three triply degenerate intermediate PESs on approach to $D_2$. Two of these PESs have $^3A''$ symmetry and one has $^3A'$, but for reasons that we return to below, only one of the $^3A''$ surfaces is expected to be reactive.[6] One $^3A''$ and one $^3A'$ surface therefore propagate through the saddle-point region and correlate with the $OD(X^2\Pi) + D(^2S)$ ground-state products. These 8-fold degenerate products also correlate with electronically excited $O(^1D) + D_2$ reactants via a $^1A'$ surface, which cuts through the

**Received:** June 8, 2014
**Published:** August 1, 2014

   dx.doi.org/10.1021/ja505743c | *J. Am. Chem. Soc.* 2014, 136, 12371−12384

triplet surfaces and cannot be ignored if spin−orbit coupling is non-negligible, and with a higher excited singlet state via a $^1A''$ surface. The overall situation is illustrated schematically in Figure 1.

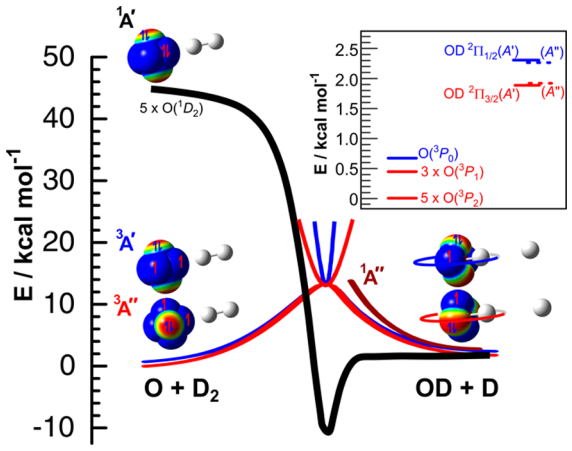


**Figure 1.** Schematic representation of the multiple potential energy curves that play a role in the dynamics of the $O(^3P)$ + $H_2$ (or $D_2$) reaction. The inset shows the fine-structure splittings of reactant and product states.

At low levels of rotation, $OD(X^2\Pi)$ is reasonably well described by Hund's case (a) coupling into a pair of well-separated spin−orbit manifolds, with a splitting of around 130 $cm^{-1}$ (0.4 kcal $mol^{-1}$), labeled $^2\Pi_{3/2}$ and $^2\Pi_{1/2}$ or $F_1$ and $F_2$, respectively. This description is increasingly approximate for higher rotational levels: we return to the significance of this below. As is normal practice, we shall use the Hund's case (b) notation, $N$ (the angular momentum quantum number excluding spin), to label the rotational levels. Within each spin−orbit manifold, every level is further split into two parities or Λ-doublets, $\Pi(A')$ and $\Pi(A'')$, labeled to indicate their opposite high-$N$-limiting reflection symmetries with respect to the plane in which the OD molecule is rotating.[37] Although the splitting between Λ-doublet levels is small, at most only a few $cm^{-1}$ for levels that are relevant here, selection rules fortunately make it easy to resolve them spectroscopically. The measured populations of the fine-structure and Λ-doublet levels therefore potentially act as signatures of the symmetries of the surfaces over which reaction propagates and the non-adiabatic couplings between them.

The first "chemically accurate" pair of $^3A'$ and $^3A''$ surfaces, with estimated average errors of 0.3 kcal $mol^{-1}$, was obtained by Rogers, Wang, Kuppermann, and Walch (RWKW) using complete active space self-consistent field (CASSCF) with correlation-consistent polarized valence quintuple (cc-pV5Z) basis sets.[11] These have become the benchmark PESs for this reaction and have been used in a wide range of subsequent scattering studies, including quasi classical trajectory (QCT), time-independent and time-dependent wavepacket quantum scattering (QS), and various semiclassical methods.[10,12−15,17−30,32] The $^3A''$ RWKW surface was extended to longer range by Brandão et al.,[16] and at least one other set of PESs has recently been published,[31] which has not yet been tested extensively through scattering calculations. The equivalent benchmark singlet surfaces, including the $^1A'$ surface correlating to $O(^1D)$ + $H_2$ reactants which will be relevant below in the discussion of spin−orbit coupling, were calculated by Dobbyn and Knowles (DK) using CASSCF and multi reference configuration interaction (MRCI) methods.[38] The most significant development in the treatment of the coupling of the triplet and singlet surfaces is the reduced-dimensional four-state model of Hoffmann and Schatz.[10] We return to this model in detail, along with the subsequent scattering calculations on the coupled surfaces, when we compare the corresponding theoretical results with our experimental results below.

A key feature of the RWKW and earlier realistic $O(^3P)$ + $H_2$ PESs is the high barrier of around 10 kcal $mol^{-1}$. This is consistent with the very small thermal rate constants except at elevated temperatures.[1,9,18,23] The high barrier, along with the unfavorable kinematics, also explains the great imbalance noted above between the number of theoretical treatments of the dynamics and successful attempts to study them experimentally. Prior to the development and application to this system of the hyperthermal $O(^3P)$ source,[12,22] which is also used in the current work, the only partly successful approach was based on the alternative method of providing the energy to the reactants partially in the form of $H_2$ vibration.[39] However, the signal strengths were insufficient for the authors of this study to measure nascent OH product-state distributions by laser-induced fluorescence (LIF) under single-collision conditions.

The hyperthermal $O(^3P)$ source has been used successfully in conjunction with universal rotating mass-spectrometric detection to measure the excitation function for the $O(^3P)$ + $H_2$ reaction and differential cross sections and kinetic energy release for the $O(^3P)$ + $D_2$ reaction (selected for kinematic reasons).[12,22] Among other key findings was the observation that a large fraction, around ∼50% on average, of the available energy must be deposited in internal energy of the OD. A high level of rotation in the ground vibrational state of OD ($v' = 0$) (adopting the usual convention that primes indicate product levels) was confirmed in our own recent report most closely related to the current work, in which LIF detection was combined for the first time with the hyperthermal $O(^3P)$ source.[40]

We substantially extend here what is known about the $O(^3P)$ + $D_2$ system by measuring the detailed rotational, fine-structure, and Λ-doublet product-state distributions across the full range of accessible OD vibrational product states, $v' = 0−2$, for a collision energy of 25 kcal $mol^{-1}$. The effects of collision energy are also examined through measurements of the $v' = 0$ rotational distributions at reduced energies of 20 and 15 kcal $mol^{-1}$. We present a much fuller analysis of the agreement, and some significant discrepancies related to electronically non-adiabatic effects, between the experimental results and the results of prevailing theory. We suggest a possible source of at least one of the serious disagreements.

## 2. EXPERIMENTAL DETAILS

The experiment was performed with the use of a crossed-molecular-beams apparatus equipped with a hyperthermal atomic-oxygen beam source and laser-induced fluorescence (LIF) detection. The details of the hyperthermal beam source and the experimental setup have been described earlier.[22,40] The pulsed hyperthermal atomic-oxygen beam was crossed at right angles with a pulsed supersonic beam of $D_2$. Both beams operated at a repetition rate of 2 Hz.

The hyperthermal atomic-oxygen beam was produced with a laser-detonation source based on the original design of Caledonia et al.[41] A piezoelectric pulsed valve introduced a high-pressure (3700 kPa backing pressure) surge (approximately 100 μs long) of pure $O_2$ gas into a conical nozzle. Following a 160−170 μs delay, a 6.5 J/pulse $CO_2$


dx.doi.org/10.1021/ja505743c | J. Am. Chem. Soc. 2014, 136, 12371−12384

TEA laser was fired. The IR laser light at 10.6 $\mu$m passed through an antireflection coated ZnSe window into the source chamber where it was focused into the nozzle using a bare gold mirror of 1 m radius of curvature. The concentrated laser pulse initiated a breakdown of the gas and heated the resulting plasma to more than 40 000 K. The detonation wave dissociated and accelerated the oxygen gas in the conical nozzle (10 cm long, 20°-included angle). The resulting beam pulse contained both atomic and molecular oxygen, traveling at hyperthermal velocities in the range ∼6−9 km $s^{-1}$. The beam passed through a 3 mm diameter skimmer located 82 cm from the apex of the conical nozzle before reaching the main scattering chamber. A differentially pumped mass spectrometer was used for beam characterization. The O atom beam had a peak velocity of ∼7500 m $s^{-1}$ and a velocity spread (full width at half-maximum, fwhm) of ∼2000 m $s^{-1}$. The mole fraction of atomic oxygen in the beam was ∼80%, with the balance being $O_2$.

The $D_2$ beam was created using a piezoelectric pulsed valve, with a nozzle diameter of 1.0 mm. The backing pressure of pure $D_2$ was held at ∼280 kPa. The pulsed beam traveled 8 mm from the nozzle of the pulsed valve before passing through a 1.8 mm skimmer into the main scattering chamber. The nominal $D_2$ beam velocity was estimated to be ∼2100 m $s^{-1}$.[42] The crossing region of the two beams (interaction region) was 94 cm from the apex of the laser-detonation nozzle cone and 10.0 cm from the $D_2$ pulsed-valve nozzle.

The OD product was detected by LIF on the well-known OD($A^2\Sigma^+ \leftarrow X^2\Pi$) transition. The probe pulses were the second-harmonic output of a tunable dye laser (Continuum ND6000) pumped by a 532 nm Nd:YAG laser (Continuum Surelite III). The probe laser pulse had a nominal line width of 0.16 $cm^{-1}$ and a temporal length of 5 ns. The probe beam was linearly polarized in the vertical direction in the laboratory, perpendicular to the plane of the molecular beams and along the direction of fluorescence detection. It intersected the interaction region in the collision plane, bisecting the O atom and $D_2$ beams at 45°. A combination of a half-wave plate and a Glan−Taylor polarizer was used to control the probe laser pulse energy while maintaining fixed linear polarization. Brewster-angle entrance and exit windows on the main chamber were used to maximize transmission and reduce the scattered laser light.

Fluorescence was collected perpendicular to the plane containing the laser beam and the molecular beams using a telescope arrangement consisting of two $f$ = 5 cm positive lenses, each with a diameter of 5 cm. The emission passed through an appropriate narrow-band-pass filter to isolate the selected OD A−X vibronic band (see below) and to discriminate against scattered laser light. The transmitted light was detected by a photomultiplier tube (PMT, Electron Tubes 9813-QB). A part of the probe laser beam was reflected onto a photodiode before entry into the chamber to monitor the relative pulse energy. The photodiode signal and the fluorescence signal were averaged and integrated using an oscilloscope (Tektronix TDS 3044B) and captured on a computer. The corresponding wavelength was recorded simultaneously.

The probe laser was synchronized with the atomic-oxygen and $D_2$ beams in such a way that the nominal collision energy at which the OD product was formed could be controlled with high precision. For the current study, the probe laser passed the interaction region at the precise moment that O atoms with a velocity of 7800, 6900, or 5900 m $s^{-1}$ in the laboratory frame arrived there, corresponding to center-of-mass (c.m.) collision energies of 25, 20, and 15 kcal $mol^{-1}$. Given the range of possible OD product velocities in the laboratory frame and the finite dimensions of the molecular beams and the probe laser beam, there will be some contribution from OD products that are formed at earlier times from O atoms with correspondingly higher velocities. These velocities are distributed in a way that is not straightforward to estimate precisely, but nevertheless, it is not difficult to show that the resulting spread is relatively small. The majority of the products will have exited the viewing region after traveling a small multiple (less than a factor of ∼2) of the probe beam radius. A minor fraction will recoil along the probe-beam-propagation axis and hence in principle remain available to be excited for longer times, but even in that case, they are quickly discriminated against by the low-$f$ collection optics. It has previously been established[22] that the majority of the products are backscattered in the c.m. frame, with ∼50% on average of the available energy in kinetic energy (consistent with the rotational distributions that we measure here). This corresponds to molecules traveling at ∼5500 $ms^{-1}$ in the laboratory frame. They therefore traverse the nominal ∼3 mm distance needed to escape from the center of the probe beam in ∼1.0 $\mu$s. This is only 0.5% of the total flight time of 120 $\mu$s of the O atoms from the source to the scattering region. The corresponding spread in O + $D_2$ collision energies is ∼1.0%, or around 0.25 kcal $mol^{-1}$.

During the acquisition of a typical fluorescence excitation spectrum, the OD LIF signal was averaged over 32 pulses at each probe-laser wavelength, which was scanned with an increment of 0.001 nm. Each excitation spectrum was collected three times at $E_{coll}$ = 25 kcal $mol^{-1}$ and once each at the reduced energies of $E_{coll}$ = 20 and 15 kcal $mol^{-1}$. The OD products in $v'$ = 0 were excited on the A−X(1,0) band, and the fluorescence was collected on the (1,1) band using a narrow bandpass filter (fwhm = 12 nm) centered at 313 nm. This combination helped to reduce the background from scattered laser light. For these measurements, the probe laser was scanned from ∼287 to 293.5 nm. The OD products in $v'$ = 1, 2 were excited using (1,1) and (2,2) diagonal bands, respectively, and the fluorescence was collected on the corresponding (1,0) and (2,1) bands using a narrow band-pass filter (fwhm = 20 nm) centered at 289 nm. Observation of fluorescence on these off-diagonal transitions again helped to reduce the background from scattered laser light. For these measurements, the probe laser was scanned from ∼310.5 to 320 nm. Typical values of the laser pulse energies at the point of entry to the chamber, for the 25 kcal $mol^{-1}$ collision energy, were 100−130 $\mu$J for probing OD $v'$ = 0 and 1 and ∼200 $\mu$J for probing $v'$ = 2, with an unfocused beam diameter of ∼6 mm. The pulse energy was maintained at ∼100 $\mu$J when probing $v'$ = 0 at the reduced collision energy of 20 kcal $mol^{-1}$ but increased to ∼330 $\mu$J to accommodate the smaller signals at 15 kcal $mol^{-1}$.

We did not search for LIF signals originating from OD $v'$ = 3. This would be awkward experimentally because of the non-negligible rotational-level-dependent predissociation in $v$ = 3 of the OD(A) state if the A−X(3,3) diagonal band were to be used.[43] However, at the highest collision energy of 25 kcal $mol^{-1}$, the threshold for OD $v'$ = 3 production lies only 1.3 kcal $mol^{-1}$ below the total energy available. The previous crossed-beam scattering experiments[22] at this collision energy implied that <1% of the products had a translational energy of less than 1.3 kcal $mol^{-1}$. Similarly, the theoretical prediction[22] was of only 0.3% (QCT) or <0.01% (QS) of the population appearing in OD $v'$ = 3. We therefore conclude that the neglect of this channel will not significantly affect the assessment of the overall product branching. The excitation spectra were analyzed on the assumption (whose validity is explored below) of a linear regime in which intensities and hence populations are directly proportional to the probe-laser pulse energy and to the absorption coefficient of the corresponding transition in absorption. Intensities were corrected for the measured fluctuations in laser energy and O-beam intensity during the scan. The corrected spectrum was imported and fitted with the use of the spectrum-simulation software, LIFBase,[43] from which the desired rotational population distributions were obtained. Further corrections were applied for filter transmission and PMT detection sensitivity, accounting for the known wavelengths and line strengths for all the lines in emission from the specific upper state accessed by each transition in absorption. The LIFBase simulation accounts for the reduction in the fluorescence quantum yield due to predissociation in the OD(A) state. This is completely negligible for $N$ < 25 and $N$ < 7 in the relevant two upper-state vibronic levels $v$ = 1 and 2, respectively (see above). Even for the highest levels accessed here, the correction applied for the reduced quantum yield was <4% for $v$ = 1, $N$ = 28 and <8% for $v$ = 2, $N$ = 18. As a cross-check on the reliability of the fitting procedure, we manually analyzed the ratios of populations from pairs of main Q and P or R lines which happen to be accidentally close to each other in the spectrum. The areas of the peaks were fitted using Gaussian functions. After application of the corrections for absorption coefficients and branch-weighted detection sensitivities, we obtained

population ratios that, averaged over eight pairs of lines, agreed within 20% with those derived using LIFBase.

As discussed at length in our previous report,[40] we were conscious of the possible distortion of measured population ratios due to the effects of either optical saturation or laboratory-frame alignment of the rotational angular momentum of the OD products. We therefore do not repeat all the details of that analysis but summarize only the essential outcomes and explain how they may have affected the more extended relative population measurements reported here.

Optical saturation will in all cases have had relatively little effect on distributions over $N'$ within a given vibrational level because of the slow variation of the absorption coefficients within a single branch of a given band in the excitation spectrum. Similarly, they are unlikely to significantly distort measured $F_1/F_2$ spin−orbit ratios because these are obtained from branch pairs ($R_1/R_2$ or $Q_1/Q_2$) that also have very similar line strengths.

Saturation is potentially more significant for the $\Pi(A')/\Pi(A'')$ Λ-doublet ratios, because the branch pairs used ($R_1/Q_1$ or $R_2/Q_2$) have high-$N$-limiting line strengths in the ratio ∼1:2. As discussed previously,[40] for the estimated absolute laser fluences used to probe OD $v' = 0$ on the (1,0) band, the *a priori* expectation would be of possible moderate saturation. The main-branch to satellite-branch ratios are a much more sensitive indicator of saturation because of the substantially larger ratios of line strengths than those between main branches. These were found for $E_{coll}$ = 25 kcal mol$^{-1}$ to be not significantly different from the ratios of line strengths for $R_1/R_{21}$ pairs, and only clearly systematically distorted for $Q_1/Q_{21}$ pairs which have the most extreme ratios (up to 40:1 for the levels probed in these cross-checks). We therefore concluded that optical saturation would have had only a minor, if any, effect on measured Λ-doublet ratios for OD $v' = 0$ at 25 kcal mol$^{-1}$.[40] This would be equally true for $v' = 0$ at $E_{coll}$ = 20 kcal mol$^{-1}$ here, for which similar pulse energies were used. Saturation may have been somewhat more significant at $E_{coll}$ = 15 kcal mol$^{-1}$, where the probe fluence was increased by a factor of ∼3. Conclusions on Λ-doublet populations might not be made so confidently from these lowest-energy data alone. Similarly, the $v' = 1$ data obtained with comparable pulse energies to those used for the $v' = 0$ would also be, if anything, more saturated because the absorption coefficients are around a factor of ∼2.5 larger on the (1,1) band than on the (1,0) band. Any saturation of the (2,2) band would be similar to (1,1), because the lower absorption coefficients, more similar to those of the (1,0) band, are effectively compensated by the higher pulse energies used. Note that, in all cases where saturation is significant, any systematic distortion would be to *increase* the apparent $\Pi(A')/\Pi(A'')$ ratio because the R-branches would be less saturated than the Q-branches.

Similar arguments apply to vibrational branching ratios, where whichever is the weaker band in absorption would be systematically favored in a partially saturated regime. As we explain below, we used overlapping lines in the (2,1):(1,0) and (2,2):(1,1) band pairs to assess the $v' = 1/v' = 0$ and $v' = 2/v' = 1$ ratios, respectively. The more extreme of the cases is the (2,1):(1,0) pair, because the absorption coefficients are in the ratio of ∼1:6. As noted above, the strengths of the (2,2) and (1,1) bands are more similar, differing by less than a factor of 2.

The effects of laboratory-frame alignment of the OD product rotational vectors on apparent population ratios cannot be assessed definitively without prior knowledge of the stereodynamics, which are currently unexplored experimentally. However, where common branch types are used to measure relative populations, any stereodynamic factors will be very similar. Therefore, the only potentially significant effect will again be on measured $\Pi(A')/\Pi(A'')$ Λ-doublet ratios obtained from comparison of R- and Q-branches. As we have discussed at length previously,[40] the effects of linear laser polarization on the measured LIF intensities on different branches from an aligned sample can be expressed in the formalism of Greene and Zare[44] as

$$I(J_i \rightarrow J_e; \chi_a) = CS_{J_i \rightarrow J_e} \sum_{J_f} \{f_d S_{J_e \rightarrow J_f} \sum_{k_d,k_a,k} [A_0^{(k)} \overline{g}^{(k)} \overline{g}^{(k_d)} \times \omega(k_d, k_a, k; J_i, J_e, J_f) \sum_{\chi_d = 0,\pi/2} \varepsilon(k_d, k_a, k, 0; \chi_a, \chi_d)]\} \quad (1)$$

where the symbols have their usual meanings and are defined in the Supporting Information of ref 40. It is convenient to simplify eq 1 by factoring out the population and the line strength of the probe transition to define a "polarization sensitivity", $D(J_i)$. This is an implicit function of the branch type of the $J_i \rightarrow J_e$ probe transition, suitably summed and weighted over the $J_e \rightarrow J_f$ branches detected and the unresolved polarization of the emission. $D(J_i)$ is defined through

$$P_{app}(J_i) = D(J_i) P_{true}(J_i) \quad (2)$$

where $P_{app}(J_i)$ is the apparent relative population in level $J_i$ measured from a true population, $P_{true}(J_i)$, via the standard analysis of the LIF excitation spectrum assuming a linear dependence on the absorption coefficient in absorption.

$D(J_i)$ depends on the known geometric parameters, including the direction of linear polarization of the probe beam. This was deliberately chosen in our experiments to point toward the detector, because this minimizes the variation of $D(J_i)$ with branch type. The stereodynamical information is contained in the values of the alignment parameters, $A_0^{(2)}$ and $A_0^{(4)}$. Although these are experimentally unknown, the value of $A_0^{(2)}$ has been estimated theoretically to be −0.83.[27,30] This is close to the dynamical limit of −1 that would result from $j'$ being strictly perpendicular to the initial relative velocity, $k$ (which is the axis of cylindrical symmetry in the experiment). A value for $A_0^{(4)}$ was not reported by Xu and Zong,[27] but an approximate value can be estimated by assuming that the value of $A_0^{(2)}$ is the result of a single mean value of the angle between $j'$ and $k$. This gives $A_0^{(4)} = \sim +0.18$, which is about half the maximally aligned limit.

In assessing the values of $D(J_i)$, we have taken the Xu and Zong result as one limit and the other as the completely isotropic case of no laboratory-frame alignment of OD. As is well-known from the work of Greene and Zare,[44] $D(J_i) \neq 1$ even in the isotropic case. The effects of probe polarization are always relatively modest for an isotropic sample, though: in our geometry, R-branches are slightly favored, with $D(J_i) \leq 1.07$, relative to Q-branches, $D(J_i) \geq 0.87$. For the negative alignment predicted by Xu and Zong, the sense of the preference is reversed and somewhat larger: for R-branches, $D(J_i) \geq 0.84$, and for Q-branches, $D(J_i) \leq 1.20$. (Full $J_i$-dependent results are given in the Supporting Information to ref 40. $D(J_i)$ always approaches unity at very low $J_i$ because of nuclear-hyperfine depolarization, incorporated in eq 1 through the factors $\overline{g}^{(k)}$ and $\overline{g}^{(k_d)}$.)

If the sample were isotropic in the laboratory frame, then the measured $\Pi(A')/\Pi(A'')$ Λ-doublet ratios could be *over*estimated, by up to around 20%. If the theoretical predictions are correct, though, and the OD is negatively aligned, then the $\Pi(A')/\Pi(A'')$ ratio could be *under*estimated, by up to 40%.

## 3. RESULTS

**3.1. Full Rovibrational Product-State Distributions at $E_{coll}$ = 25 kcal mol$^{-1}$.** The rovibrational populations across the full set of accessible vibrational levels $v' = 0$, 1, and 2 were measured at the highest collision energy of 25 kcal mol$^{-1}$. A representative LIF excitation spectrum for OD $v' = 1$ excited on the (1,1) band, along with the fit from simulation, is shown in Figure 2. The rotational assignments of the three main branches ($R_1$, $Q_1$, and $P_1$) originating from the $F_1$ manifold are shown to help give a visual indication of the level of rotational excitation. The labels on the main branches from $F_2$ and the satellite branches are omitted for clarity.


dx.doi.org/10.1021/ja505743c | J. Am. Chem. Soc. 2014, 136, 12371−12384

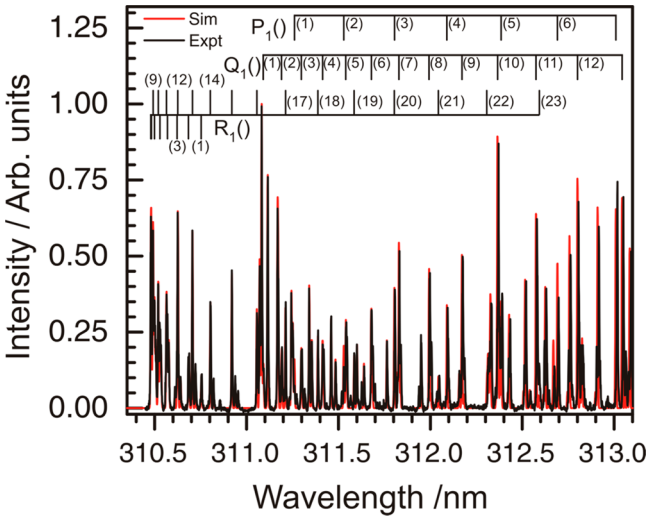


**Figure 2.** OD A–X(1,1) LIF excitation spectrum of the $v'$ = 1 products of the $O(^3P)$ + $D_2$ reaction at $E_{coll}$ = 25 kcal mol$^{-1}$. Experimental data (black spectrum) and simulation from which populations were extracted (red spectrum). The experimental spectrum has been corrected for variations in probe laser energy with wavelength. The positions of the main branch lines are indicated, labeled by the quantum number, $N'$.

The populations extracted from the spectra for each of the observed vibrational levels are collected in Figure 3. Results derived from the $R_1$, $R_2$, $Q_1$, and $Q_2$ branches are shown separately, in each case normalized to the most populated discrete rotational level within a vibrational level. We have discussed in detail above and elsewhere[40] why we believe that these apparent population ratios within single branches are not significantly affected by artifacts resulting from either optical saturation in the probe step or laboratory-frame alignment of the OD products. The error bars are obtained from the statistical variation in three independent measurements of the excitation spectrum.

There is clearly a high level of OD rotational excitation, extending in each case out to the total energetic limit of 23.1 kcal mol$^{-1}$ set by the collision energy of 25 kcal mol$^{-1}$ and the modest (1.9 kcal mol$^{-1}$) endothermicity of the reaction. As expected for a total-energy constraint, the peak and maximum rotational levels decline with vibrational level. Table 1 lists the average energies appearing in rotation, $\langle E_{rot} \rangle$, for each of the vibrational levels, averaged over the contributing spin–orbit and lambda-doublet levels. The results are also expressed as average fractions, $\langle f_{rot} \rangle$, of the remaining energy available to rotation for a given vibrational level, $E_{avl}(v')$.

Fortuitously, there are lines of the (2,1) band that appear within the same wavelength region as the (1,0) band. Similarly, the (1,1) and (2,2) bands are partially overlapping. Knowing the rotational distributions for $v'$ = 0 and 1, the relative intensities of selected lines in the (2,1) and (1,0) transitions were used to obtain relative populations in $v'$ = 0 and 1. Averaged over four independent spectra at $E_{coll}$ = 25 kcal mol$^{-1}$, the $v'$ = 0:$v'$ = 1 ratio was estimated to be 0.83 ± 0.03:0.16 ± 0.03. In line with the discussion above, any effect of partial saturation would be for this ratio to be an underestimate, because $v'$ = 0 was probed on the stronger (1,0) band. Laboratory-frame alignment in this case would not be a factor because common branch types were compared.

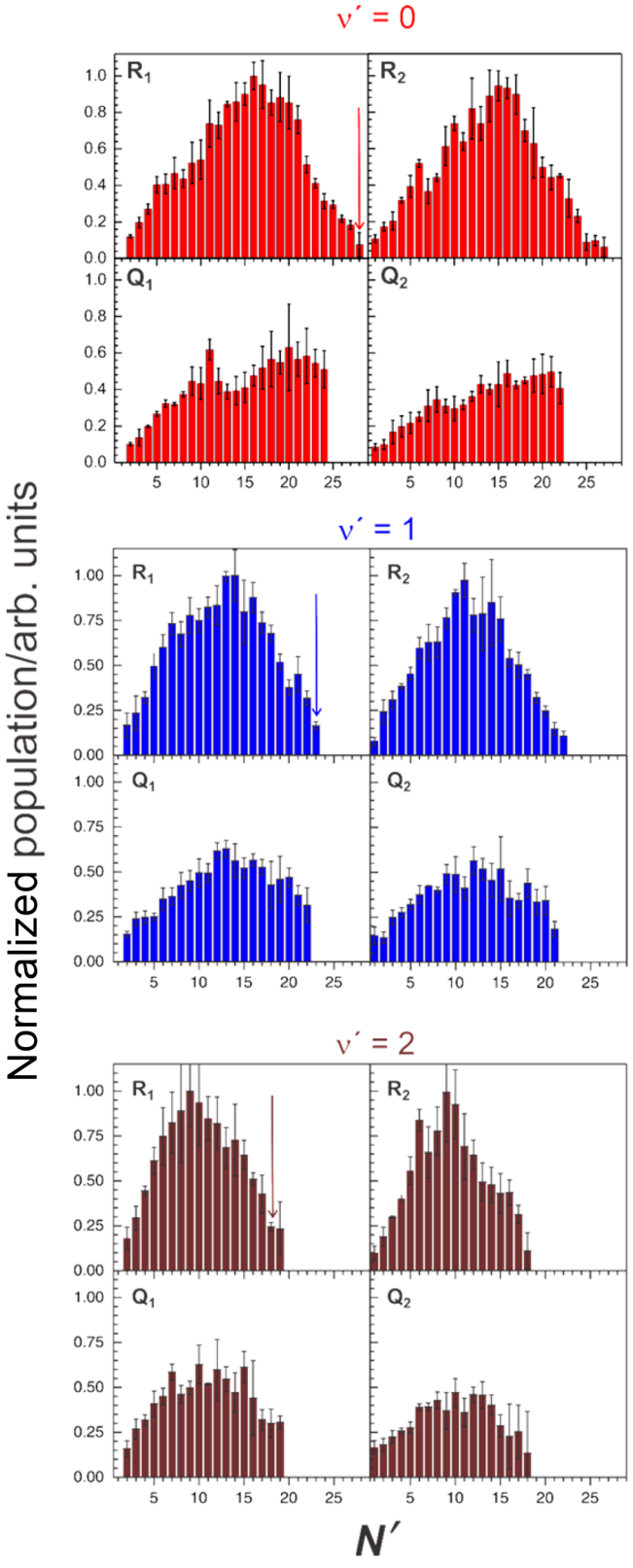


**Figure 3.** Rotational distributions of OD in $v'$ = 0, 1, and 2 (red, blue, and brown, respectively) at $E_{coll}$ = 25 kcal mol$^{-1}$. The maximum rotational excitation allowed for OD in $v'$ = 0, 1, and 2 is $N'$ = 28, 23, and 17, respectively, as indicated by the arrows.

Similarly, using the rotational distributions for $v'$ = 1 and 2 along with relative intensities of overlapping lines in the (1,1) and (2,2) bands, the average $v'$ = 1:$v'$ = 2 ratio over three


dx.doi.org/10.1021/ja505743c | J. Am. Chem. Soc. 2014, 136, 12371–12384

**Table 1. Average Rotational Energies in the Observed OD Vibrational Levels[a]**

| | $v' = 0$ | | | $v' = 1$ | | | $v' = 2$ | | |
|---|---|---|---|---|---|---|---|---|---|
| $E_{coll}$ | $E_{avl}(v')^b$ | $\langle E_{rot}\rangle$ | $\langle f_{rot}\rangle^c$ | $E_{avl}(v')^b$ | $\langle E_{rot}\rangle$ | $\langle f_{rot}\rangle^c$ | $E_{avl}(v')^b$ | $\langle E_{rot}\rangle$ | $\langle f_{rot}\rangle^c$ |
| 25 | 23 | 8.8[d] | 0.38[d] | 15.5 | 6.7 | 0.43 | 8.2 | 4.9 | 0.60 |
| 20 | 18 | 7.4 | 0.41 | | | | | | |
| 15 | 13 | 4.01 | 0.40 | | | | | | |

[a]All energies in kcal mol$^{-1}$. [b]$E_{avl}(v') = E_{coll} - (\Delta_r H) - E(v')$. [c]$\langle f_{rot}\rangle = \langle E_{rot}\rangle / E_{avl}(v')$. [d]$\langle E_{rot}\rangle$ and $\langle f_{rot}\rangle$ are likely to be slightly underestimated for $v' = 0$ at $E_{col} = 25$ kcal mol$^{-1}$ due to the unobserved populations in the highest rotational levels.

independent spectra at 25 kcal mol$^{-1}$ was 0.78 ± 0.01:0.22 ± 0.01. Hence, the overall normalized branching ratio into OD $v'$ = 0, 1, and 2 was 0.80:0.16:0.04. The corresponding average energy appearing in vibration, $\langle E_{vib}\rangle$, is therefore only 1.8 kcal mol$^{-1}$, equivalent to an average fraction, $\langle f_{vib}\rangle$, of 8% of the available energy. If we use the vibrational branching ratio to weight the vibrational-level-dependent average rotational energy in Table 1, we find an overall average energy in rotation of 8.3 kcal mol$^{-1}$ and fraction of the available energy, $\langle f_{rot}\rangle$, of 0.36.

The format of Figure 3 allows the spin−orbit (i.e., $R_1/R_2$ or $Q_1/Q_2$) or Λ-doublet (i.e., $R_1/Q_1$ or $R_2/Q_2$) population ratios to be assessed visually. It can be seen immediately that any differences between spin−orbit manifolds are slight, but there is a clear and consistent preference for the Π(A′) Λ-doublet, probed by the R branches, across all three vibrational levels.

These trends are highlighted in Figures 4 and 5. Figure 4 shows the relative populations in the two spin−orbit manifolds, averaged over the Λ-doublets, as a function of rotational level for each vibrational level. Any preference for either $F_1$ or $F_2$ is slight across the greater part of the range with significant population. There is some tendency for $F_1$ to be favored, particularly in the higher rotational levels, but this may not be statistically significant given the relatively large error limits associated with the declining populations in these levels. As discussed above, these results would be insensitive to either optical saturation or laboratory-frame polarization.

In contrast, Figure 5 demonstrates the consistent net preference for the Π(A′) Λ-doublet across all three vibrational levels. Although subject to some statistical scatter, this shows a very similar pattern for all vibrational levels. Unsurprisingly, for well-known dynamical and spectroscopic reasons (see below), the Π(A′)/Π(A″) ratio is initially near unity in the lowest rotational levels. It then builds to a broad maximum with a value of ∼2 in the region of the peak of the vibrational-level-dependent rotational distribution, before declining in all cases to near unity in the highest levels.

As discussed above, if these apparent ratios had been artifacts resulting from optical saturation, then the Π(A′)/Π(A″) ratios should appear higher for $v' = 1$ and 2 because they were obtained using stronger diagonal bands and/or higher pulse energies than the (1,0) band used for $v' = 0$. There is no clear sign of such an effect in Figure 5. Furthermore, as we have noted previously,[40] the observation of an artificial Π(A′)/Π(A″) ratio with a peak value of ∼2 would require the transitions to be *totally* saturated. Selected measurements at higher pulse energies showed that more significant saturation could be induced and it could not therefore have been complete under the conditions in which the $v' = 0$ data were recorded.[40] There is also no obvious reason why the Π(A′)/Π(A″) ratio should artificially vary within one vibrational band because the ratio of R- to Q-branch line strengths is not strongly $N$-dependent beyond the first few levels.

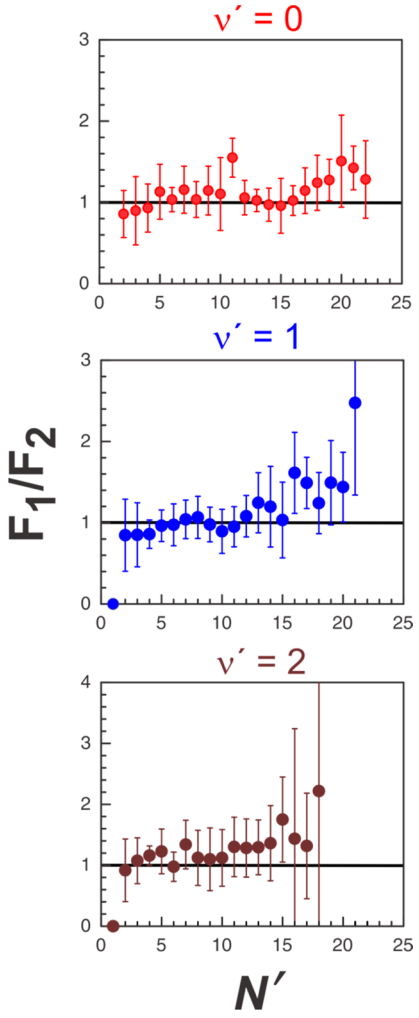


**Figure 4.** Spin−orbit ratio of product OD in $v' = 0$, 1, and 2 at $E_{coll}$ = 25 kcal mol$^{-1}$.

As we have also noted above, an artificially high Π(A′)/Π(A″) ratio could result from polarization effects if the OD rotation is isotropic in the laboratory frame. The magnitude of such an effect is limited, though, to around 20%, and could not in itself explain the significantly larger peak preference observed here. On the other hand, if the OD rotation is actually negatively aligned, as theoretically predicted,[27] the measured Π(A′)/Π(A″) ratio is an *under*estimate, by up to 40%, compounding the observed preference for Π(A′).

**3.2. The Effects of Collision Energy on the Rotational Distribution in OD $v' = 0$.** We have explored the collision energy dependence of the rotational energy disposal in the dominant OD $v' = 0$ vibrational level. More restricted measurements of the (1,0) LIF excitation spectra were carried out at successively lower collision energies of 20 and 15 kcal


dx.doi.org/10.1021/ja505743c | J. Am. Chem. Soc. 2014, 136, 12371−12384

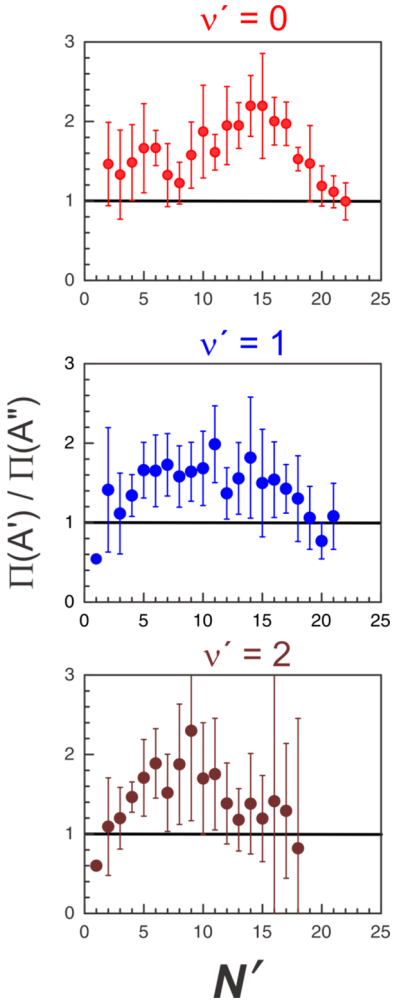


**Figure 5.** Λ-doublet ratio of product OD in $v'$ = 0, 1, and 2 at $E_{coll}$ = 25 kcal mol$^{-1}$.

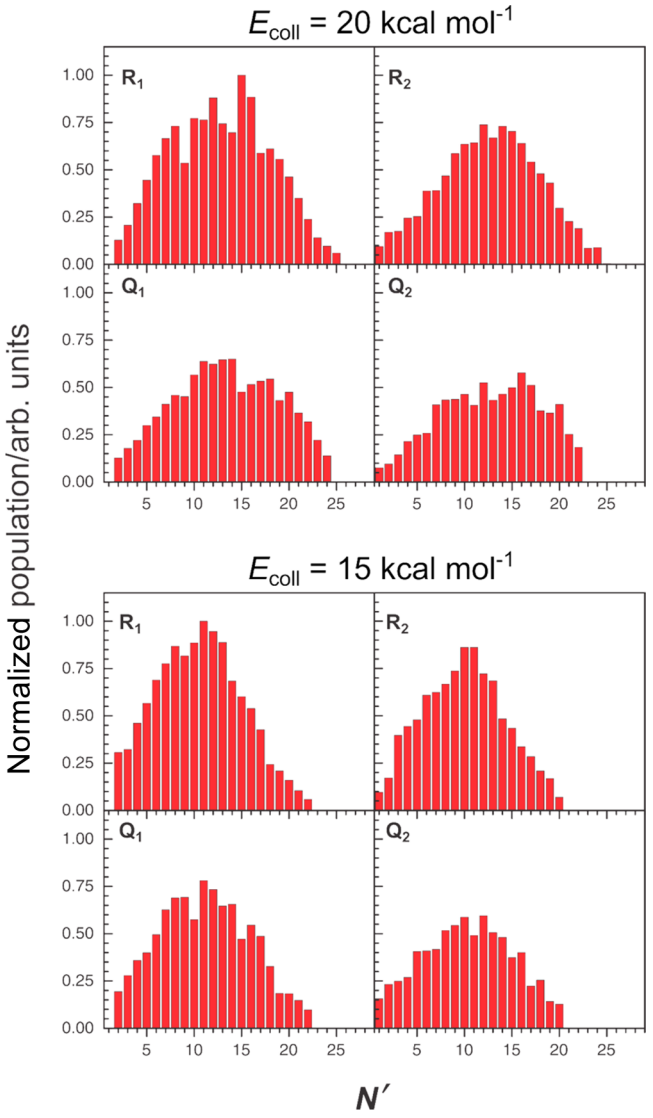


**Figure 6.** Rotational distributions of OD in $v'$ = 0 for $E_{coll}$ = 20 and 15 kcal mol$^{-1}$.

mol$^{-1}$. The OD number density declined substantially as a result of the known reduction in the reaction cross section at lower collision energies.[12] To recover satisfactory LIF signals, the probe-laser pulse energy was increased, as noted above, to 300 $\mu$J at $E_{coll}$ = 15 kcal mol$^{-1}$. As we have explored above, this will have had little effect on the overall rotational populations and also on the spin−orbit branching, but it may result in some systematic bias in the apparent Λ-doublet ratios.

The branch-dependent populations, peak-normalized within each vibrational level, are shown in Figure 6. The general patterns are similar to those in the upper panel of Figure 3 other than, as expected, lower levels of rotational excitation as the collision energy is reduced. These trends are illustrated clearly in the overall rotational distributions averaged over spin−orbit and Λ-doublet levels for all three collision energies in Figure 7. The corresponding values of $\langle E_{rot}\rangle$ and $\langle f_{rot}\rangle$ are included in Table 1.

As at the higher collision energy of 25 kcal mol$^{-1}$, the branch-dependent data in Figure 6 contain the $N'$-dependent spin−orbit and Λ-doublet ratios. The spin−orbit ratios, averaged over Λ-doublet levels, are collected for all three collision energies in Figure 8. Although the statistics are poorer at the lower collision energies, they appear to confirm a persistent modest preference for the lower, $F_1$, spin−orbit manifold, which may also be present at 25 kcal mol$^{-1}$.

The collision-energy-dependent Λ-doublet ratios are shown in Figure 9. The clear preference for the Π(A′) levels that was noted for $E_{coll}$ = 25 kcal mol$^{-1}$ appears to still be present for the lower energy of 20 kcal mol$^{-1}$ but may be somewhat reduced. The drop in the Π(A′)/Π(A″) ratio at the highest rotational levels is also present but is similarly less pronounced. These general trends continue with the further reduction to $E_{coll}$ = 15 kcal mol$^{-1}$, where there may even be a reversal of the preference in the highest $N'$ levels. As indicated above, these data may be less reliable than those at the higher collision energies due to a higher degree of optical saturation, but note that this would have had the effect of *increasing* the apparent Π(A′)/Π(A″) ratio, rather than decreasing it as is observed.

## 4. DISCUSSION

**4.1. Rovibrational Populations.** The results in Figure 3 show that the substantial rotational energy release observed in our more restricted previous measurements[40] on OD $v'$ = 0 extends to all accessible vibrational levels. The successive decline in rotational excitation in $v'$ = 1 and 2 is, of course, expected from a total-energy constraint. As Table 1 shows,


dx.doi.org/10.1021/ja505743c | J. Am. Chem. Soc. 2014, 136, 12371−12384

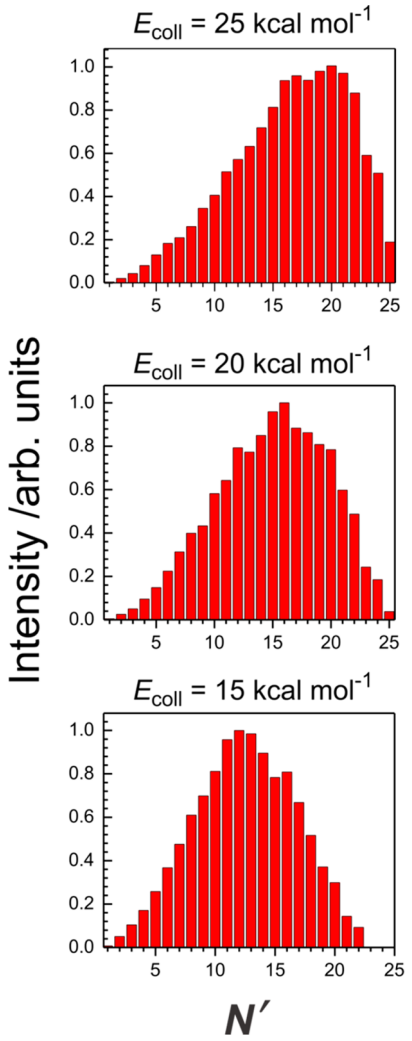


**Figure 7.** Overall rotational distribution (averaged over $R_1$, $R_2$, $Q_1$, and $Q_2$ branches) of OD in $v' = 0$ at $E_{coll}$ = 25, 20, and 15 kcal mol$^{-1}$.

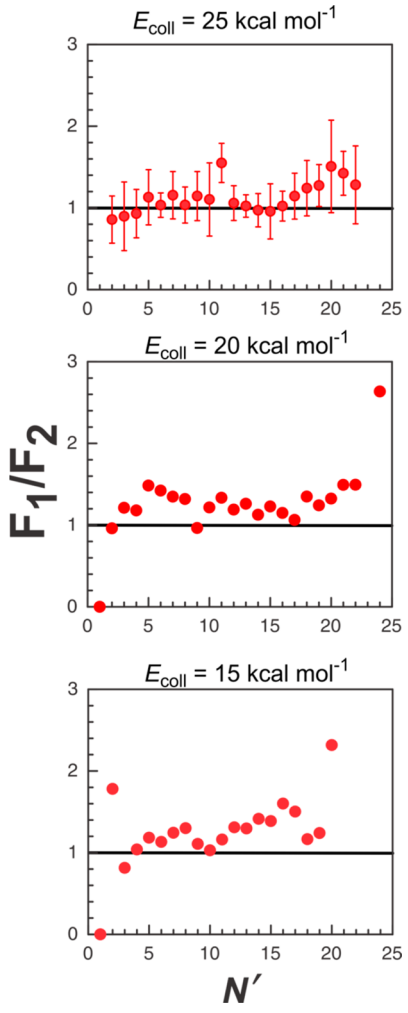


**Figure 8.** Spin−orbit ratios of product OD in $v' = 0$ at $E_{coll}$ = 25, 20, and 15 kcal mol$^{-1}$.

though, when expressed as a fraction of the residual total energy available for each vibrational level, a higher proportion is channeled into OD rotation than relative translation. We also show here for the first time (Figures 6 and 7) that the absolute level of rotational excitation in OD $v' = 0$ declines with the collision energy, but when expressed as a fraction of the available energy, it is almost constant (Table 1).

The observed significant levels of rotational excitation (with a vibrational-weighted fraction of energy in rotation of 36% at 25 kcal mol$^{-1}$) agrees with the qualitatively hot (but non-nascent) rotational distributions in OH $v' = 0$ found previously from the reaction, $O(^3P) + H_2(v' = 1)$.[39] They are also reproduced well in quantum scattering calculations on the RWKW surfaces by Schatz and co-workers,[22] as illustrated in Figure 10. The scattering calculations[22] also correctly predict the relatively low levels of OD vibrational excitation that we observe experimentally, with only slightly less quantitative accuracy than the rotational distributions (see Figure 10). Theory suggests $v'$ = 0:1:2 ratios of 0.72:0.25:0.03 at 25 kcal mol$^{-1}$, whereas we observe 0.80:0.16:0.04. The overall average internal energy release of 8% in vibration and 36% in rotation that we observe is also broadly consistent with the ∼50% deduced from the earlier crossed-beam measurements of kinetic energy release.[22]

All of these observations therefore suggest that the theoretical description provided by the RWKW surfaces is essentially correct, at least in terms of their ability to reproduce the mechanical forces experienced by the atoms. The basic picture of direct dynamics through a preferred collinear minimum energy path, but with significant excursions to wider angles because of the high collision energy, therefore appears to be correct. Repulsive energy release through bent O−D−D configurations is quite efficiently converted to asymptotic rotation of OD because of the kinematics. Consistent with well-established principles of Polanyi's rules, the relatively central barrier location combined with heavy + light−light kinematics does not efficiently convert the available energy into OD vibration.

**4.2. Spin−Orbit Populations.** As Figure 4 shows, there is little, if any, statistically significant deviation from unity in the observed $F_1/F_2$ ratios across all three vibrational levels of OD $v'$ = 0, 1, and 2 at a collision energy of 25 kcal mol$^{-1}$. Any systematic variation that is present is an increase in the $F_1/F_2$ ratio at high $N'$, but generally not beyond the estimated statistical uncertainties which become rapidly larger as the populations in both levels fall. This absence of a clear spin−orbit preference also persists across the range of collision energies, as demonstrated in Figure 8.


dx.doi.org/10.1021/ja505743c | J. Am. Chem. Soc. 2014, 136, 12371−12384

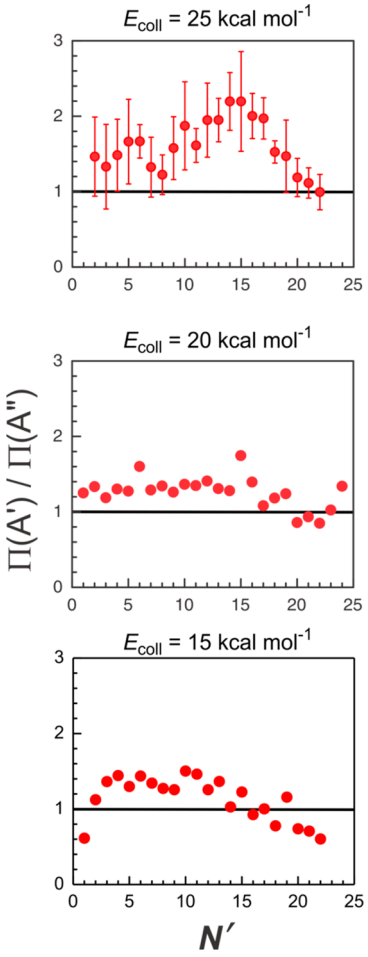


**Figure 9.** Λ-doublet ratios of product OD in $v' = 0$ at $E_{coll}$ = 25, 20, and 15 kcal mol$^{-1}$. Note the comment in the text about the degree of optical saturation for the 15 kcal mol$^{-1}$ data.

Unlike the mechanical rotational distributions, this observation is in striking contrast to almost all the existing theoretical predictions. All recent serious attempts to predict the spin−orbit branching ratio in OH (or OD) from O($^3$P) + $H_2$ (or $D_2$) build on the analysis of Hoffmann and Schatz.[10] These authors recognized that the full dimensionality of the spin−orbit-coupled multisurface problem of O($^3$P) and O($^1$D) reacting with $H_2$ (or $D_2$) made it intractable, at least with the methods and computational resources available at that time. The full problem has a 9-fold degeneracy associated with the O($^3$P) + $H_2$ asymptote and 5-fold for O($^1$D) + $H_2$. Hoffmann and Schatz set about reducing this dimensionality, as we explain below. The reason that the singlet surfaces correlating asymptotically with O($^1$D) + $H_2$ cannot necessarily be ignored in a treatment of the ground-state O($^3$P) + $H_2$ reaction is, of course, that the lowest, $1^1$A′, singlet surface is deeply bound. Even in moderately bent O−H−H geometries, based on the DK and RWKW surfaces, respectively, the $1^1$A′ surface crosses the reactive triplet surfaces correlating with O($^3$P) + $H_2$ on the reactant side of the barrier. This is indicated schematically in Figure 1. Figure 11a outlines more fully the complete set of surfaces correlating with both reactants and products.

Hoffmann and Schatz excluded from their basis all other high-lying singlet surfaces. From the perspective of the reactants, this approximation is reasonable because the next-highest surface, $1^1$A″, lies at much higher energy. However, this is at the expense of not including the $^1$A″ surface which is needed in a full, 8-fold-degenerate description of the OH($X^2\Pi$) + H($^2$S) product asymptote. They also excluded the $2^3$A″ entrance-channel surface, on the elementary grounds[6] that it is associated with an occupancy in which a filled p-orbital is directed toward the incoming $H_2$ molecule and hence is unreactive.

The remaining surfaces were shown by Hoffmann and Schatz to fall into two symmetry blocks, with no spin−orbit coupling between blocks. In a symmetry-adapted Cartesian representation, the surfaces $^3A_x''$, $^3A_y''$, and $^3A_z'$ couple among themselves and also to the $^1$A′ surface. The remaining three surfaces, $^3A_z''$, $^3A_x'$, and $^3A_y'$, also mutually couple but *not* to $^1$A′ (although they would, in principle, couple to the $^1$A″ surface needed for a full description of the products). Recognizing their focus on singlet−triplet intersystem crossing, Hoffmann and Schatz retained only the 4-fold block $^3A_x''$, $^3A_y''$, $^3A_z'$, and $^1$A′. These states could then be represented by the available RWKW $^3$A″ (twice) and $^3A_z'$ surfaces and the DK $^1$A′ surface, respectively. The spin−orbit coupling matrix elements between these surfaces were obtained from CASSCF calculations using the effective-nuclear-charge, one-electron Breit−Pauli expression.

This overall process of elimination is shown schematically in Figure 11b. Note that one important consequence is that the true (5-, 3-, and 1-fold) degeneracy of the $^3P_J$ entrance-channel states is lost, being replaced in the model with three singly degenerate triplet levels. Nevertheless, it has been common practice in reporting subsequent scattering calculations to continue to refer to these levels using the original $^3P_2$, $^3P_1$, and $^3P_0$ labels. The product asymptote is not affected to the same extent, because the $^3A_x''$, $^3A_y''$, $^3A_z'$, and $^1$A′ basis generates, correctly, two pairs of degenerate levels that can be associated with the splitting into $^2\Pi_{3/2}$ and $^2\Pi_{1/2}$ manifolds in OH, although the true 8-fold degeneracy of H($^2$S) + OH($X^2\Pi$) is again lost.

The trajectory-surface hopping (TSH) scattering calculations published alongside the derivation of the four-state model by Hoffmann and Schatz[10] were not designed to address the question of the spin−orbit branching in the OH product. They were carried out in a diabatic basis that does not properly describe the splittings in the asymptotic reactant or product regions. This aspect was first addressed in the subsequent work of Maiti and Schatz.[13] TSH calculations in a new mixed representation, with smooth switching between adiabatic asymptotes and diabatic intermediate geometries, found a clear preference for O($^3$P) + $H_2$ to populate the $^2\Pi_{3/2}$ state of OH. This essentially reflects the fact that within the four-state model the dynamics are predominantly adiabatic, and only modestly affected, to an extent of around ∼10%, by non-adiabatic transitions induced by spin−orbit coupling. The lower two entrance-channel triplet states, at least nominally labeled as $^3P_2$ and $^3P_1$ (see above), consequently produce primarily the lower states of the product, associated with OH $^2\Pi_{3/2}$. Conversely, the highest ($^3P_0$) reactant state produces primarily OH $^2\Pi_{1/2}$. This has been shown not to be an artifact of the TSH method in subsequent calculations using alternative time-dependent quantum scattering methods by Han and co-workers[19,20,25] and by others.[26−28,31,32]

The only apparent exception to this essential result was found in the intervening semiclassical calculations using trajectory dynamics within the approximate-quantum-potential approach, developed by Garashchuk, Rassolov, and Schatz.[21]


dx.doi.org/10.1021/ja505743c | J. Am. Chem. Soc. 2014, 136, 12371−12384

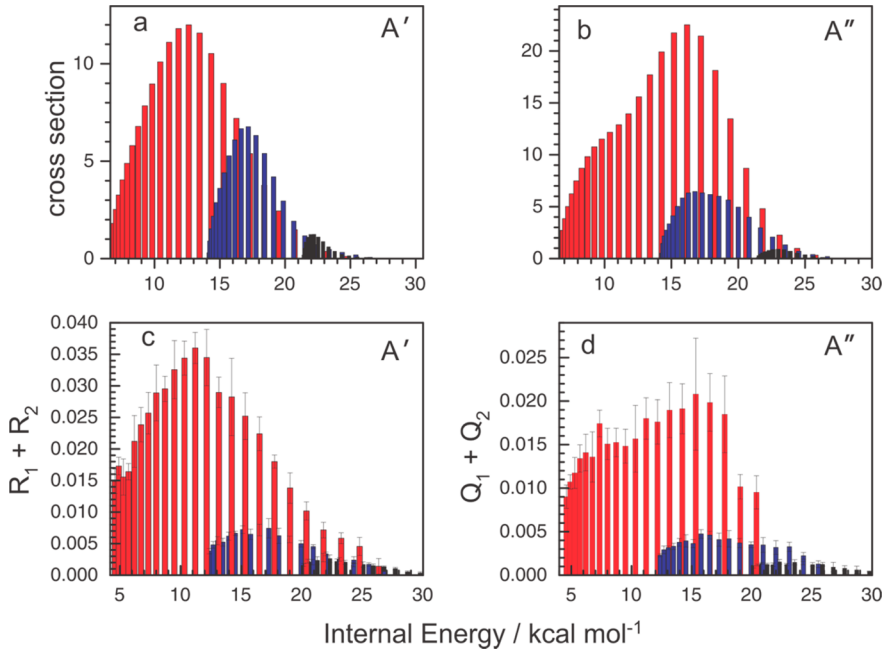


**Figure 10.** Comparison of (a and b) theoretically predicted (QS) and (c and d) experimentally observed rovibrational distributions of product OD in the reaction at $E_{coll}$ = 25 kcal mol$^{-1}$ ($v$ = 0 in red, $v$ = 1 in blue, and $v$ = 2 in black bars). Parts a and b represent calculated reaction cross sections on the $^3$A′ and $^3$A″ surfaces, taken from ref 22. Parts c and d are the experimentally observed Λ-doublet-resolved product-state distributions averaged over the $F_1$ and $F_2$ spin−orbit manifolds.

Much more nearly equal $^2\Pi_{3/2}$ and $^2\Pi_{1/2}$ populations were predicted starting from any of the reactant states. However, we believe from an analysis of their detailed methodology that this was a consequence of an asymmetrical treatment of the entrance and exit channels. The calculations were carried out in a diabatic basis, with the appropriate projection onto adiabatic final states being imposed on the product side. However, the corresponding transformation was not carried out for the reactant states, which were defined in terms of single *diabatic* states, rather than as their complex combinations necessary to describe single *adiabatic* states. This does not therefore overturn the near-adiabatic behavior found in all other studies.

At least two conceptual problems arise in trying to compare the overall OH spin−orbit preference predicted from any of the calculations using the Hoffmann and Schatz four-state model quantitatively with those from our experiments. The first is that the theoretically predicted populations represent the branching between asymptotic $^2\Pi_{3/2}$ and $^2\Pi_{1/2}$ surfaces split by the spin−orbit interaction in the rotationless OD (or OH) molecule. However, the experiments detect the relative populations in the true, spectroscopic $F_1$ and $F_2$ states. These would only be uniquely associated with $^2\Pi_{3/2}$ and $^2\Pi_{1/2}$ states in the strict Hund's case (a) limit. This applies only approximately to the lowest levels of OD (or OH), which have partial Hund's case (b) character that increases significantly with $N$. The true states are linear combinations of the case (a) wave functions:

$$|F_1\rangle = a_j|^2\Pi_{3/2}\rangle + b_j|^2\Pi_{1/2}\rangle \quad (3)$$

$$|F_2\rangle = -b_j|^2\Pi_{3/2}\rangle + a_j|^2\Pi_{1/2}\rangle \quad (4)$$

where the $N$-dependent mixing coefficients, $a_j$ and $b_j$, are well-known and can be calculated from closed-form expressions[45] involving the rotational and spin−orbit splitting constants, or from diagonalization of the full Hamiltonian.[46] We find essentially identical numerical results from either approach. To illustrate the effects of this decoupling, we list in Table 2 the $F_1/F_2$ ratios that would be observed for underlying case (a) $^2\Pi_{3/2}/^2\Pi_{1/2}$ ratios of 2 and 8, chosen as limiting cases for reasons that we return to shortly, using the constants for OD $v'$ = 0. The result is, of course, a decline in the $F_1/F_2$ ratio with $N$, but even the lower underlying spin−orbit ratio of 2 is not damped to what would be unobservable levels across the more heavily populated levels: this can be seen by comparing Table 2 with Figures 3 and 4. Moreover, as noted above, any trend in Figure 4, across all three product vibrational levels, is the opposite of the decrease in the $F_1/F_2$ ratio with $N'$ that results from decoupling. We do not therefore believe that decoupling alone could be responsible for the failure to observe experimentally the $^2\Pi_{3/2}$ preference predicted from the Hoffmann and Schatz four-state model.

The second problem arises in the choice of weighting of the reactant states. The true $^3P_2$, $^3P_1$, and $^3P_0$ reactant states in the experiments will have relative populations very close to 5:3:1 because of the very high effective temperature in the laser-detonation source. If these degeneracies are used to weight the results on the three different entrance-channel states in the four-state model, then the predicted $^2\Pi_{3/2}/^2\Pi_{1/2}$ spin−orbit ratio will be ∼8, because of the near-adiabaticity noted above. This is clearly very different from the experimental result. If, alternatively, the nondegeneracy of the model entrance-channel states is used, then the $^2\Pi_{3/2}/^2\Pi_{1/2}$ ratio will be ∼2, at least somewhat closer to experiment. This is the weighting used (in advance of the experiments) by Maiti and Schatz.[13] They noted that the predicted ratio was in good agreement with the then available experimental results for the related O($^3$P) + saturated hydrocarbon reactions.[47,48] Because of the lower collision energies in those experiments, the O($^3$P) + hydrocarbon reactions can be expected to be dominated by near-collinear geometries. This is also supported by up-to-date *ab initio* potential energy surfaces and QCT scattering calculations on


dx.doi.org/10.1021/ja505743c | J. Am. Chem. Soc. 2014, 136, 12371−12384

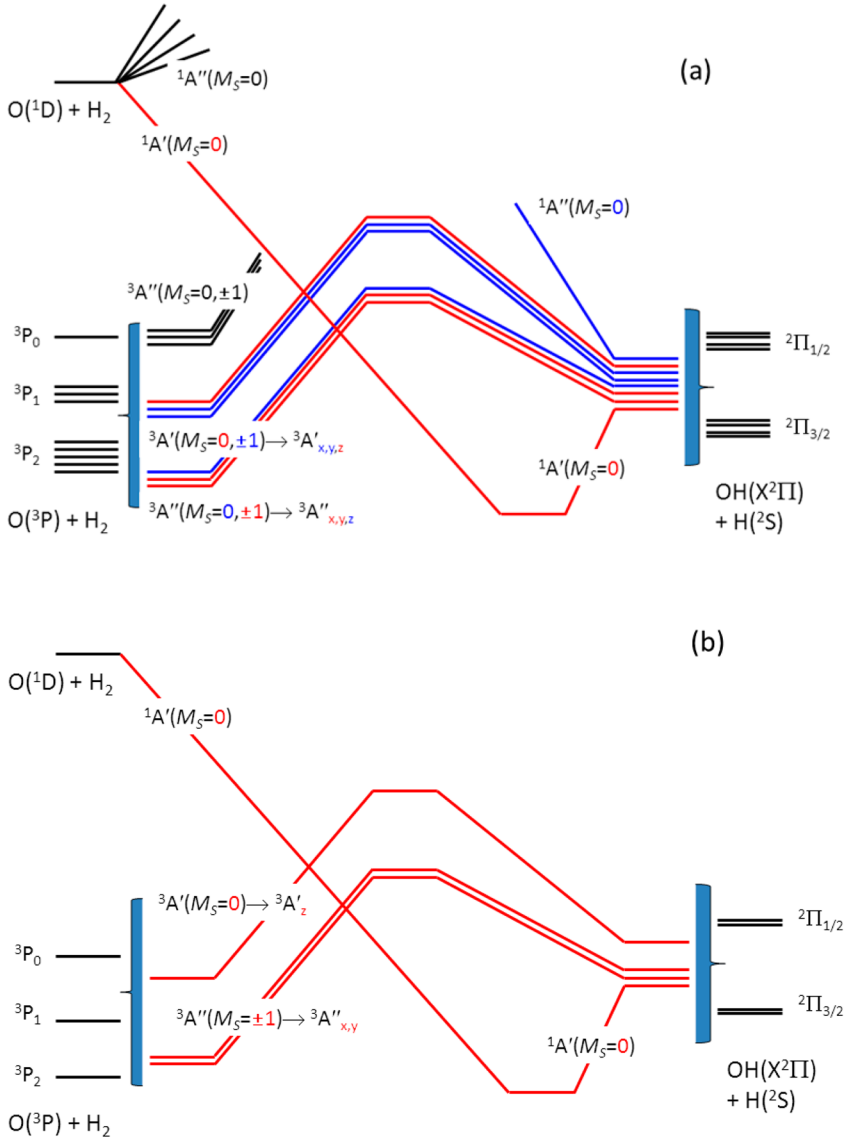


**Figure 11.** Schematic potential energy surfaces in the reaction of $O(^3P)$ and $O(^1D)$ with $H_2$ (or $D_2$). (a) The full set of reactant and ground-state product surfaces. Surfaces in black are excluded in the Hoffmann and Schatz[10] four-state model for energetic reasons, and those in blue, on the grounds of symmetry. (b) The surfaces retained in the four-state model. Note the reduced degeneracies of the reactant and product asymptotes.

**Table 2. OD $F_1/F_2$ Ratios for Assumed Underlying $^2\Pi_{3/2}/^2\Pi_{1/2}$ Ratios, Accounting for *N*-Dependent Hund's Case (a)/(b) Mixing**

| | $^2\Pi_{3/2}/^2\Pi_{1/2}$ ratio | |
|---|---|---|
| *N* | 2.0 | 8.0 |
| 1 | 1.99 | 7.92 |
| 5 | 1.77 | 4.84 |
| 10 | 1.51 | 2.85 |
| 15 | 1.36 | 2.13 |
| 20 | 1.28 | 1.80 |
| 25 | 1.22 | 1.61 |
| 30 | 1.19 | 1.50 |

the reaction with $CH_4$.[49] A partially adiabatic model based on correlations in collinear geometries did successfully reproduce the observed preference for $^2\Pi_{3/2}$ products.[48]

The absence of a similar preference for OD $^2\Pi_{3/2}$ from $O(^3P)$ + $D_2$ is unlikely to be a result of the change of isotope: the spin−orbit ratios for $O(^3P)$ + deuterated hydrocarbons are essentially identical to those with normal hydrogen,[50] and quantum scattering indicates that non-adiabaticity is only modestly larger for $O(^3P)$ + $D_2$ than for $H_2$.[32]

We are led therefore to question the basic construction of the Hoffmann and Schatz four-state model[10] as the inherent source of the discrepancy with experiment. Maiti and Schatz[13] did consider explicitly the possible effects of having excluded the $^3A_z''$, $^3A_x'$, and $^3A_y'$ three-state triplet block (recall Figure 11) on the spin−orbit branching. They concluded that if these surfaces had been included they would have produced a similar $^2\Pi_{3/2}/^2\Pi_{1/2}$ ratio to those in the four-state block. However, because two of the states in the omitted three-state block have $^3A'$ symmetry and only one is $^3A''$, we believe that the correct result of assumed near-adiabatic behavior is that the *upper* $^2\Pi_{1/2}$ spin−orbit state would be favored by a factor of ∼2:1. This would, to a first approximation, cancel out the preference for $^2\Pi_{3/2}$ from the four-state block. The result would be a *near unity* $^2\Pi_{3/2}/^2\Pi_{1/2}$ ratio, in much better agreement with experiment.


dx.doi.org/10.1021/ja505743c | J. Am. Chem. Soc. 2014, 136, 12371−12384

We would therefore strongly encourage further theoretical exploration of the spin−orbit branching, ideally without any artificial reduction in the number of entrance-channel surfaces treated. This would allow the correct inclusion of any significant coupling between surfaces in the entrance channel, including the nonreactive $2^3A''$ surface, in the important region where the electrostatic splitting is of the same order as the asymptotic spin−orbit splitting. It would also eliminate the issue of the nonphysical degeneracies of the reactant states. Similarly, retention of the $^1A''$ surface on the product side would allow mixing between electrostatic surfaces in the separating products and also recover their correct, 8-fold degeneracy.

**4.3. Λ-Doublet Populations.** The more extensive results here confirm our previous initial observation,[40] confined to $v' = 0$, that there is an overall clear preference for the OD $^2\Pi(A')$ Λ-doublet. We note that a qualitatively similar preference was reported from the earlier experiments of Weiner and co-workers on $O(^3P) + H_2(v = 1)$, despite the non-nascent conditions.[39] The pattern we find here is consistent across all OD vibrational levels at a collision energy of 25 kcal mol$^{-1}$, as shown in Figure 5. The $^2\Pi(A')/^2\Pi(A'')$ ratio peaks at ∼2:1 in the vicinity of the maximum in the OD rotational distribution. It declines, as expected, to near unity at low $N'$. This is required dynamically because of the corresponding reduction in the degree of electron alignment.[51] Interestingly, it also declines at high $N'$, where there is no similar generic dynamical constraint. This general pattern also persists at lower collision energies (Figure 9), although, with less statistical certainty, it may possibly be less pronounced. We have considered carefully the effects of both optical saturation and laboratory-frame alignment of the OD rotation as possible sources of an artificial preference for $^2\Pi(A')$, but we conclude that they do not offer a consistent explanation for the observations. Even in a worst-case scenario where the spectra are all much more heavily saturated than had been realized, the corresponding lower-limiting $^2\Pi(A')/^2\Pi(A'')$ ratio would be around unity.

We stress that there have been, as yet, no rigorous theoretical attempts to predict the OD (or OH) Λ-doublet ratios for the $O(^3P) + D_2$ (or $H_2$) reaction. Nevertheless, it is possible to speculate qualitatively on the consequences of the relative reaction cross sections on the RWKW $^3A'$ and $^3A''$ surfaces obtained by Schatz and co-workers.[22] Single-surface QCT and time-independent quantum scattering (CCH) calculations are in generally good agreement. The CCH prediction is that the cross section is significantly larger, by a factor of ∼2, on the $^3A''$ surface. This is a direct consequence of the less-steep bending curve on this surface in the vicinity of the saddle point,[6,11] allowing a wider range of angles to contribute to the reactivity at a given collision energy. In the limit that the reaction is sufficiently sudden that the plane of the three atoms at the saddle point coincides with the final plane of rotation of the OD product, the reflection symmetry of the Λ-doublet product will be a signature of the surface on which it was formed. However, this simple argument would predict a preference for the $^2\Pi(A'')$ Λ-doublet which is the *opposite* of the experimental observation. The experimental decline in the $^2\Pi(A')/^2\Pi(A'')$ ratio at high $N'$ could conceivably be interpreted as consistent with this effect coming into play for the most rotationally excited products, but the overall preference for $^2\Pi(A')$ products at lower $N'$ would remain unexplained.

This dilemma is explored eloquently in a commentary by Alexander on our initial report on this reaction.[52] As he explains, there is a limit in which the $^2\Pi(A')$ product will be favored by a statistical factor of around 2, first identified explicitly by Bronikowski and Zare.[53] In a collinear approach geometry, the unpaired orbital lobe lies along a direction perpendicular to the $z$ axis taken to coincide with the approach or (antiparallel) recoil direction (i.e., $k$ and $k'$ in the usual notation). For simple geometric reasons, if the OD product rotates with equal probability around Cartesian $x$ and $y$ axes perpendicular to $z$, then OD $^2\Pi(A')$ and $^2\Pi(A'')$ products will be produced with equal probability. This is what is expected in a sudden limit in which bending in planes corresponding to $^3A'$ and $^3A''$ surfaces is equally likely. Moreover, rotation *around* $z$ also results in production of the $^2\Pi(A')$ Λ-doublet. If this is also equally probable, then the 2:1 ratio in favor of $^2\Pi(A')$ is obtained.

However, dynamically, rotation around $z$ will not be generated by repulsion between the separating OD and D fragments. A Coriolis-type mechanism is required to couple out-of-plane tumbling motion of the three-atom O−D−D transient complex into final rotation of OD. There may be some indication of whether the stereodynamics of the reaction are compatible with this mechanism in the classical QCT scattering calculations of Xu and Zong for the $O(^3P) + H_2$ system.[27] In agreement with the earlier experiments and copublished scattering calculations of Garton et al.,[22] Xu and Zong predict a differential cross section ($P_{00}$ in the polarization-dependent differential cross sections (PDDCS) notation that they use) that is predominantly backward for OD scattering on both the $^3A'$ and $^3A''$ RWKW surfaces. Interestingly, however, the scattering may be somewhat more sideways on the $^3A''$ surface, particularly toward the highest energy of 25 kcal mol$^{-1}$ corresponding to the majority of our measurements here. Therefore, it is only approximately the case that the $z$ axis in the Alexander model coincides with initial and final relative velocity vectors, $k$ and $k'$. Nevertheless, Xu and Zong find that OH rotational alignment ($P_{20}$), implicitly integrated over all final rotational states, is not far from its limiting value of −0.5 in the region where the differential cross section has significant intensity. This implies that $j'$ is quite strongly perpendicular to $k$ and, to the extent that $k$ and $k'$ are antiparallel, also perpendicular to $k'$. This limit, which is incompatible with the rotation needed to generate the $^2\Pi(A')$ preference in the Alexander model, is again approached less closely on the $^3A''$ surface. Xu and Zong's three-vector correlation, $P_{22}+$, is also broadly compatible with $j'$ being largely perpendicular to $k$, and in the plane perpendicular to the scattering plane defined by $k$ and $k'$. However, this is once again more true for the $^3A'$ than $^3A''$ surface, and substantially breaks down at a relatively high collision energy of 25 kcal mol$^{-1}$ on both surfaces.

Xu and Zong's results do not therefore necessarily rule out the possibility of some rotation about $z$ being responsible for the reversal of the Λ-doublet preference in the Alexander model. This may be particularly effective if the $^3A'$ surface behaves closer to the in-plane repulsive-recoil limit, helping to preserve its own preference for $^2\Pi(A')$ products, whereas the $A''$ surface deviates more from this limit, tending to scramble the $^2\Pi(A'')$ products that would otherwise have been produced.

All of these speculative propositions clearly require proper testing by rigorous, rotational-state-resolved scattering calculations. Ideally, these would be carried out on the full set of coupled surfaces also necessary to treat the spin−orbit branching, as discussed above. Moreover, such calculations would necessarily lead to predictions about other potentially

interesting aspects of the stereodynamics which could, in principle, be tested by future experiments. However, the challenge in carrying out such calculations should not be understated, because of the large number of surfaces involved combined with the high collision energy needed to overcome the barrier. This would require a large number of basis functions, particularly for the deeply bound $1^1A'$ surface.

## 5. CONCLUSION

The reaction of atomic oxygen $O(^3P)$ with $D_2$ leads to relatively highly rotationally and moderately vibrationally excited OD. These distributions are successfully reproduced in QCT and QS scattering calculations,[22] suggesting that the mechanical forces experienced by the atoms are well-described by the accepted lowest $^3A'$ and $^3A''$ surfaces.[11] However, the absence of a clear preference for either OD spin−orbit state is at odds with QCT surface-hopping[13] or time-dependent wavepacket scattering[19,20,25,32] calculations (QS) on the four-surface model of Hoffmann and Schatz.[10] We suggest that this may be an intrinsic feature of this reduced-dimensional model and encourage further theoretical exploration. The observation of a consistent $N'$-dependent preference for the $^2\Pi(A')$ Λ-doublet across all product vibrational levels remains to be explained satisfactorily and is also an outstanding challenge to theory.[52]

## AUTHOR INFORMATION


### Corresponding Authors

tminton@montana.edu

k.g.mckendrick@hw.ac.uk


### Notes

The authors declare no competing financial interest.

## ACKNOWLEDGMENTS

This work has been supported by the Air Force Office of Scientific Research: FA9550-10-1-0563. K.G.M. is grateful for a Royal Society Leverhulme Trust Senior Research Fellowship under which this work was initiated. We are grateful to Prof. George C. Schatz and Dr. Biswajit Maiti for many helpful discussions. We also appreciate the helpful input from discussions with Dr. Matthew Costen, Prof. Keli Han, and Dr. Peiyu Zhang. The data described in this work can be obtained from the corresponding authors on request.

## REFERENCES


(1) Tsang, W.; Hampson, R. F. *J. Phys. Chem. Ref. Data* **1986**, *15*, 1087.

(2) Spaans, M.; Tielens, A. G. G. M.; Dishoeck, E. F. v.; Bakes, E. L. O. *Astrophys. J.* **1994**, *437*, 270.

(3) Agundez, M.; Cernicharo, J.; Goicoechea, J. R. *Astron. Astrophys.* **2008**, *483*, 831.

(4) Woitke, P.; Thi, W. F.; Kamp, I.; Hogerheijde, M. R. *Astron. Astrophys.* **2009**, *501*, L5.

(5) Sternberg, A.; Dalgarno, A. *Astrophys. J., Suppl. Ser.* **1995**, *99*, 565.

(6) Walch, S. P.; Wagner, A. F.; Dunning, T. H., Jr.; Schatz, G. C. *J. Chem. Phys.* **1980**, *72*, 2894.

(7) Schatz, G. C.; Wagner, A. F.; Walch, S. P.; Bowman, J. M. *J. Chem. Phys.* **1981**, *74*, 4984.

(8) Schatz, G. C. *J. Chem. Phys.* **1985**, *83*, 5677.

(9) Garrett, B. C.; Truhlar, D. G. *Int. J. Quantum Chem.* **1986**, *29*, 1463.

(10) Hoffmann, M. R.; Schatz, G. C. *J. Chem. Phys.* **2000**, *113*, 9456.

(11) Rogers, S.; Wang, D.; Kuppermann, A.; Walch, S. *J. Phys. Chem. A* **2000**, *104*, 2308.

(12) Garton, D. J.; Minton, T. K.; Maiti, B.; Troya, D.; Schatz, G. C. *J. Chem. Phys.* **2003**, *118*, 1585.

(13) Maiti, B.; Schatz, G. C. *J. Chem. Phys.* **2003**, *119*, 12360.

(14) Balakrishnan, N. *J. Chem. Phys.* **2003**, *119*, 195.

(15) Balakrishnan, N. *J. Chem. Phys.* **2004**, *121*, 6346.

(16) Brandao, J.; Mogo, C.; Silva, B. C. *J. Chem. Phys.* **2004**, *121*, 8861.

(17) Braunstein, M.; Adler-Golden, S.; Maiti, B.; Schatz, G. C. *J. Chem. Phys.* **2004**, *120*, 4316.

(18) Sultanov, R. A.; Balakrishnan, N. *J. Chem. Phys.* **2004**, *121*, 11038.

(19) Chu, T. S.; Zhang, X.; Han, K. L. *J. Chem. Phys.* **2005**, *122*, 214301.

(20) Chu, T.-S.; Zhang, Y.; Han, K.-L. *Int. Rev. Phys. Chem.* **2006**, *25*, 201.

(21) Garashchuk, S.; Rassolov, V. A.; Schatz, G. C. *J. Chem. Phys.* **2006**, *124*, 244307.

(22) Garton, D. J.; Brunsvold, A. L.; Minton, T. K.; Troya, D.; Maiti, B.; Schatz, G. C. *J. Phys. Chem. A* **2006**, *110*, 1327.

(23) Wang, W.; Rosa, C.; Brandao, J. *Chem. Phys. Lett.* **2006**, *418*, 250.

(24) Weck, P. F.; Balakrishnan, N.; Brandao, J.; Rosa, C.; Wang, W. *J. Chem. Phys.* **2006**, *124*, 074308.

(25) Li, B.; Han, K.-L. *J. Phys. Chem. A* **2009**, *113*, 10189.

(26) Wei, Q.; Li, X.; Li, T. *Chem. Phys.* **2010**, *368*, 58.

(27) Xu, Z.; Zong, F. *J. Mol. Struct.: THEOCHEM* **2010**, *960*, 22.

(28) Han, B.; Zheng, Y. *J. Comput. Chem.* **2011**, *32*, 3520.

(29) Liu, S.-L.; Shi, Y. *Chem. Phys. Lett.* **2011**, *501*, 197.

(30) Xu, Z.-H.; Zong, F.-J. *Chin. Phys. B* **2011**, *20*, 063104.

(31) Zhai, H.; Zhang, P.; Zhou, P. *Comput. Theor. Chem.* **2012**, *986*, 25.

(32) Zhao, J. *J. Chem. Phys.* **2013**, *138*, 134309.

(33) Che, L.; Ren, Z. F.; Wang, X. G.; Dong, W. R.; Dai, D. X.; Wang, X. Y.; Zhang, D. H.; Yang, X. M.; Sheng, L. S.; Li, G. L.; Werner, H. J.; Lique, F.; Alexander, M. H. *Science* **2007**, *317*, 1061.

(34) Lique, F.; Alexander, M. H.; Li, G.; Werner, H.-J.; Nizkorodov, S. A.; Harper, W. W.; Nesbitt, D. J. *J. Chem. Phys.* **2008**, *128*, 084313.

(35) Lique, F.; Li, G.; Werner, H.-J.; Alexander, M. H. *J. Chem. Phys.* **2011**, *134*, 231101.

(36) Jankunas, J.; Zare, R. N.; Bouakline, F.; Althorpe, S. C.; Herraez-Aguilar, D.; Aoiz, F. J. *Science* **2012**, *336*, 1687.

(37) Alexander, M. H.; Andresen, P.; Bacis, R.; Bersohn, R.; Comes, F. J.; Dagdigian, P. J.; Dixon, R. N.; Field, R. W.; Flynn, G. W.; Gericke, K.-H.; Grant, E. R.; Howard, B. J.; Huber, J. R.; King, D. S.; Kinsey, J. L.; Kleinermanns, K.; Kuchitsu, K.; Luntz, A. C.; McCaffery, A. J.; Pouilly, B.; Reisler, H.; Rosenwaks, S.; Rothe, E. W.; Shapiro, M.; Simons, J. P.; Vasudev, R.; Wiesenfeld, J. R.; Wittig, C.; Zare, R. N. *J. Chem. Phys.* **1988**, *89*, 1749.

(38) Dobbyn, A. J.; Knowles, P. J. *Mol. Phys.* **1997**, *91*, 1107.

(39) Han, J.; Chen, X.; Weiner, B. R. *Chem. Phys. Lett.* **2000**, *332*, 243.

(40) Lahankar, S. A.; Zhang, J.; McKendrick, K. G.; Minton, T. K. *Nat. Chem.* **2013**, *5*, 315.

(41) Caledonia, G. E.; Krech, R. H.; Green, B. D. *AIAA J.* **1987**, *25*, 59.

(42) Auerbach, D. J. Velocity Measurements by Time of Flight Methods. *Atomic and Molecular Beam Methods*; Oxford University Press: New York, 1988; Vol. *1*, p 362.

(43) Luque, J.; Crosley, D. R. *LIFBase*, version 1.5 ed.; SRI International Report MP 99-009; SRI International: Menlo Park, CA, 1999.

(44) Greene, C. H.; Zare, R. N. *J. Chem. Phys.* **1983**, *78*, 6741.

(45) Zare, R. N. *Angular Momentum: Understanding Spatial Aspects in Chemistry and Physics*; Wiley: New York, 1988.

(46) Stark, G.; Brault, J. W.; Abrams, M. C. *J. Opt. Soc. Am. B* **1994**, *11*, 3.

(47) Sweeney, G. M.; Watson, A.; McKendrick, K. G. *J. Chem. Phys.* **1997**, *106*, 9172.

(48) Sweeney, G. M.; McKendrick, K. G. *J. Chem. Phys.* **1997**, *106*, 9182.
(49) Gonzalez-Lavado, E.; Corchado, J. C.; Espinosa-Garcia, J. *J. Chem. Phys.* **2014**, *140*, 064310.
(50) Ausfelder, F.; Kelso, H.; McKendrick, K. G. *Phys. Chem. Chem. Phys.* **2002**, *4*, 473.
(51) Andresen, P.; Rothe, E. W. *J. Chem. Phys.* **1985**, *82*, 3634.
(52) Alexander, M. H. *Nat. Chem.* **2013**, *5*, 253.
(53) Bronikowski, M. J.; Zare, R. N. *Chem. Phys. Lett.* **1990**, *166*, 5.